Protein Engineering on Human Recombinant Follistatin: Enhancing Pharmacokinetic Characteristics for Therapeutic Application

Chuan Shen, Andrea Iskenderian, Dianna Lundberg, Tao He, Kathleen Palmieri, Robert Crooker, Qingwei Deng, Matthew Traylor, Sheng Gu, Haojing Rong, David Ehmann, Brian Pescatore, Bettina Strack-Logue, Alla Romashko, George Baviello, John Gill, Bohong Zhang, Muthuraman Meiyappan, Clark Pan, Angela W. Norton

Affiliations:

Department of Discovery Therapeutics, Shire, Lexington, MA, USA (CS, AI, DL, BP, BSL, AR, GB, JG, BZ, MM, CP, AWN)

Department of Bioanalytical and Biomarker Development, Shire, Lexington, MA, USA (TH)

Department of Discovery Biology and Translational Research, Shire, Lexington, MA, USA (KP, RC, QD, DE)

Department of Analytical Development, Shire, Lexington, MA, USA (MT, SG)

Department of Drug Metabolism & Pharmacokinetics, Shire, Lexington, MA, USA (HR)

Running title: Engineered Follistatin Molecules Enhance Pharmacokinetics

Corresponding author:

Name: Angela W. Norton
Address: Discovery Therapeutics, Shire, 300 Shire Way, Lexington, MA 02421, USA
Office phone: +1 (781) 482-0771
Fax: +1 (781) 482-2963
Email address: anorton@shire.com

Document statistics:

Number of text pages: 40 pages
Number of tables: 5
Number of figures: 5
Number of references: 45
Number of words in Abstract: 246 words
Number of words in Introduction: 722 words
Number of words in Discussion: 1499 words

A list of nonstandard abbreviations used in the paper:

AUC, area under the curve; BBXB, consensus heparin-binding motifs, B= lysine (K) or arginine (R), X= any amino acid; CHO, Chinese hamster ovary; cIEF, capillary isoelectric focusing; FS, follistatin; FS288, human follistatin 288 isoform; FS303, human follistatin 303 isoform; FS315, human follistatin 315 isoform; FS315-hFc, human follistatin 315 isoform fused with human IgG1 Fc; FSD1, follistatin domain 1; FSD2: follistatin domain 2; FSD3: follistatin domain 3; hFc, human IgG1 Fc; hFcRn, human neonatal Fc receptor; HBS, heparin binding sequence; k_a, association constant; k_d, dissociation constant; K_D, the equilibrium dissociation constant; PBS, phosphate-buffered saline; PK, pharmacokinetic; RU, response units; SPR, surface plasmon resonance; ΔHBS, HBS deficient mutant (a 12 amino acid paralogous substitution to remove heparin-binding activity)

A recommended section assignment: Drug Discovery and Translational Medicine

Abstract

Follistatin (FS) is an important regulatory protein, a natural antagonist for transforming growth factor beta family members activin and myostatin. The diverse biological roles of the activin and myostatin signaling pathways make FS a promising therapeutic target for treating human diseases exhibiting inflammation, fibrosis and muscle disorders, such as Duchenne muscular dystrophy. However, rapid heparin-mediated hepatic clearance of FS limits its therapeutic potential. We targeted the heparin binding loop of FS for site-directed mutagenesis to improve clearance parameters. By generating a series of FS variants with one, two, or three negative amino acid substitutions, we demonstrated a direct and proportional relationship between the degree of heparin binding affinity *in vitro* and the exposure *in vivo*. The triple mutation K(76,81,82)E abolished heparin binding affinity, resulting in ~20-fold improved *in vivo* exposure. This triple mutant retains full functional activity and antibody-like pharmacokinetic profile, and shows a superior developability profile in physical stability and cell productivity compared to FS variants which substitute the entire heparin binding loop with alternative sequences. Our surgical approach to mutagenesis should also reduce the immunogenicity risk. To further lower this risk, we introduced a novel glycosylation site into the heparin-binding loop. This hyperglycosylated variant showed a 10-fold improved exposure and decreased clearance in mice compared an IgG1 Fc fusion protein containing the native FS sequence. Collectively, our data highlight the importance of improving pharmacokinetic properties by manipulating heparin binding affinity and glycosylation content and provide a valuable guideline to design desirable therapeutic FS molecules.

Introduction

Follistatin (FS), a monomeric glycoprotein, was originally identified from porcine ovarian follicular fluid, and named for its ability to suppress pituitary follicle-stimulating hormone secretion (Robertson et al., 1987; Ueno et al., 1987). Subsequently, follistatin physiological function was elucidated by its inhibition of the transforming growth factor beta family members, mainly activins and myostatin (Cash et al., 2012; Hashimoto et al., 1997; Sidis et al., 2006; Welt et al., 2002). Activins participate in various biological processes, including embryonic development and growth, reproduction, energy metabolism, bone homeostasis, inflammation and fibrosis (reviewed in (Namwanje and Brown, 2016)). Myostatin, also known as growth and differentiation factor-8, is a negative regulator of myogenesis and skeletal muscle mass (reviewed in (Chen and Lee, 2016)). Myostatin inhibition significantly increases skeletal muscle mass by hypertrophy (Latres et al., 2015; Lee et al., 2005; Schuelke et al., 2004; St Andre et al., 2017). FS, by antagonism of activins and myostatin, is a promising therapeutic target for human diseases associated with inflammation, fibrosis and muscle disorders, such as Duchenne muscular dystrophy, Becker muscular dystrophy, and inclusion body myositis (Haidet et al., 2008; Kota et al., 2009; Mendell et al., 2017; Mendell et al., 2015; Rodino-Klapac et al., 2009; Walton et al., 2017).

The follistatin gene localizes on chromosome 5q11.2. Two splice variants of FS precursors exist, a 344 amino acid precursor protein and a carboxyl terminal truncated 317 amino acid precursor (Esch et al., 1987; Shimasaki et al., 1988). The first 29 amino acid residues are a putative signal sequence, translating as two N-terminal identical mature FS isoforms, FS315 and FS288. Reportedly, a third FS variant, FS303, results from proteolytic cleavage of FS315 (Sugino et al., 1993). The three isoforms play different biological roles based on differential affinities for ligands and localization. The predominant circulating isoform in human serum is FS315 (Schneyer et al., 2004), whereas FS303 predominates in ovarian follicular fluid (Sugino et al., 1993). The domain structure of FS is comprised of a 63-residue N-terminal domain, three

successive FS domains (FSD1, FSD2 and FSD3), and an acidic C-terminal tail in FS315 and

FS303 isoforms (Fig. 1). The three FS domains (~50% primary sequence homology) can be

aligned by their 10 cysteine residues. Intradomain disulfide linkages allow each FS domain

autonomous folding (Innis and Hyvonen, 2003).

FS interaction with heparin affinity columns and proteoglycan heparan sulfate on cell

surfaces was described in early characterization studies (Nakamura et al., 1991; Ueno et al.,

1987). Later studies identified a core heparin binding sequence (HBS) in FS, a highly basic 12-

residue segment (residues 75-86) located in the FSD1 domain (Innis and Hyvonen, 2003;

Inouye et al., 1992). The HBS region contains two consensus heparin-binding motifs BBXB

(Fig. 1), where B is a lysine (K) or arginine (R). Amino acid substitution in the HBS can reduce

FS binding to heparin (Sidis et al., 2005). In recent studies, an engineered FS315, with a

paralogous substitution to remove HBS fused to a murine IgG1 Fc domain, significantly

improved exposure and half-life in mice, displaying dose-dependent pharmacological effects in

a model of muscle atrophy (Datta-Mannan et al., 2013; Yaden et al., 2014). Thus,

therapeutically relevant FS variants are possible by targeting the HBS domain. To develop

desirable molecules with limited mutagenesis, and to correlate the degree of heparin binding

affinity to the pharmacokinetic behavior of recombinant FS315 fused with human IgG1 Fc

(FS315-hFc), we mutated basic residues in BBXB motifs to attain varying heparin binding

affinities. This data illustrates a direct and proportional relationship between the degree of

heparin binding *in vitro* and systemic exposure *in vivo*. We demonstrate that selective negative

charge substitutions to BBXB motifs can dramatically affect the heparin binding affinity.

During the past decade, recombinant proteins are becoming an important portion of new

biopharmaceutical products. Glycoengineering to influence the glycosylation state has been

utilized to improve recombinant protein properties such as increased stability, prolonged half-life

and decreased immunogenicity (Jefferis, 2016; Lalonde and Durocher, 2017). Introducing novel

glycosylation sites into the recombinant FS heparin-binding loop to modulate carbohydrate

content, block heparin binding and reduce the mutagenesis immunogenicity risk is largely

unexplored. In this study, we introduced new N-linked glycosylation consensus sequences

(NXT/S) into the HBS region of recombinant FS315-hFc for potential hyperglycosylation. Our

data showed that the K75N/C77T mutation effectively resulted in hyperglycosylation of the FS

fusion protein, and significantly improved *in vivo* systemic exposure.

Materials and Methods

Construction, Expression and Purification of Recombinant FS Variants. Human FS315 coding sequence was cloned from Human Liver Quick-clone cDNA (Clontech, Mountain View, CA). Human IgG1 Fc (hFc) fragment was cloned from Human Adult Normal Lung cDNA Library (Life Technology, Carlsbad, CA), and two leucine (L) residues on position 14 and 15 in the hFc region were further changed to alanine (A) by mutagenesis to reduce the affinity to Fc-gamma-receptor. FS315 and hFc fragments were subsequently cloned in frame into a mammalian expression vector. For each of the FS315-hFc variants, a mutated DNA sequence in the HBS region was synthesized by ATUM (Newark, CA), and replaced the wild type HBS region. The recombinant FS315-hFc variant plasmids were transfected into Chinese hamster ovary (CHO) cells (Sigma, St. Louis, MO) by electroporation. The cells were tested as mycoplasma free, and cultured in EX-Cell CD CHO Fusion media (Sigma) under standard condition (5% CO_2, 37°C), and selected for 10 days to generate stable pools. FS315-hFc variant proteins stably secreted in cell culture supernatant were captured onto a HiTrap MabSelect SuRe column (GE Healthcare Bio-Science, Piscataway, NJ) in 1x phosphate-buffered saline (PBS; pH 7.4), and eluted using a step-gradient of 10 mM sodium citrate (pH 2.5). The proteins were neutralized to pH 7.0 by adding 1M Tris buffer (pH 9.0). Impurities were further removed using a Superdex 200 26/600 column (GE Healthcare Bio-Science). Purity of the final proteins was >95% as analyzed by size-exclusion chromatography analysis using a Waters 2996 PDA Detector (Waters, Milford, MA).

Surface Plasmon Resonance (SPR) Binding Assay. Binding affinities of FS315-hFc variants to heparin, myostatin and human neonatal Fc receptor (hFcRn) were determined using SPR methods on a Biacore T200 instrument (GE Healthcare BioScience).

Heparin SPR Binding Assay. Biotinylated heparin (Sigma) was resuspended in 1x HBS-N buffer (10 mM HEPES, 150 mM sodium chloride, pH 7.4) and used fresh for binding studies. A

Biacore streptavidin sensor chip (GE Healthcare Bio-Science) was prepared following product instruction and biotinylated heparin was loaded to a response of approximately 40 response units (RU). All FS315-hFc samples were serially diluted in 1x HBS-EP+ buffer (10 mM HEPES, 150mM sodium chloride, 3 mM EDTA, 0.05% v/v Surfactant P20, pH 7.4) to a range of 0-25 nM for kinetic experiments. The association time and dissociation time were set to 300 s at a flow rate of 30 µl/min. Chip surface was regenerated between runs using 4 M sodium chloride. Kinetic data were fit using a 1:1 binding model.

Myostatin SPR Binding Assay. Single cycle kinetics method was used for myostatin binding. A CM5 series S sensor chip (GE Healthcare Bio-Science) with anti-hFc antibody immobilized to about 10,000 RU was used to capture all FS315-hFc variants. Myostatin (R&D Systems, Minneapolis, MN) was used as analyte in range of 0-5 nM for kinetic experiments. A 5 min association step was used for each dilution followed by a 40 min dissociation. Chip surface was regenerated using 3 M magnesium chloride between experiments.

hFcRn SPR Binding Assay. hFcRn was purified from human embryonic kidney 293 cells stably expressing hFcRn. hFcRn was immobilized on a CM5 series S sensor chip (GE Healthcare Bio-Science) with a target of approximately 500 RU. The FS315-hFc samples were serially diluted in 1x PBS-P+ buffer (20 mM phosphate buffer, 2.7 mM potassium chloride, 137 mM sodium chloride, 0.05% Surfactant P20, pH 5.5) to a range of 0-100 nM and used as analyte for multi-cycle kinetic experiments. The association and dissociation times were set at 300 s, each at a flow rate of 30 µl/min. A 1:1 binding model was used to fit the data.

Capillary Isoelectric Focusing (cIEF) Assay. The protein charge heterogeneity was monitored by cIEF analytical technique using a Peggy Sue instrument (ProteinSimple, San Jose, CA) as described by the vendor. Briefly, each of the FS315-hFc variants was diluted to 0.01 mg/ml in 10 M Urea buffer (Life Technology), diluted 4-fold with Premix/ladder mixture (ProteinSimple, San Jose, CA), and loaded 12 µl per well. Triplicates were run for each sample.

Anti-Follistatin antibody (ab47941) (Abcam, Cambridge, MA) and anti-Rabbit IgG (H&L), HRP conjugate (W4011) (Promega, Madison, WI) were diluted to 1:100 and used for detection.

SMAD-responsive Luciferase Reporter Gene Assay. The human rhabdomyosarcoma cell line A204 (HTB-82, ATCC, Manassas, VA) was stably transfected with a SMAD-responsive luciferase reporter construct pGL3(CAGA)12 as described previously (Dennler et al., 1998; Sako et al., 2010). The A204 stable cells were tested as mycoplasma free, and seeded at 40,000 cells/well/100 µl into a white corning costar 96-well plate (Corning Life Sciences, Bedford, MA) in growth medium comprised of McCoy's 5A (Life Technology), 10% dialyzed fetal bovine serum (Life Technology) and 320 µg/ml Geneticin (Life Technology) at 37°C and 5%CO_2 overnight for 16 h. The next day, 2.4 nM of myostatin (R&D Systems) or 2.4 nM of activin A (R&D Systems), and serial dilutions (1:3) of FS315-hFc variants ranging from 0-20 nM were made separately in A204 assay medium comprised of McCoy's 5A medium (HyClone, Logan, Utah) and 0.1% bovine serum albumin (ThermoFisher Scientific, Waltham, MA). Each concentration of the FS315-hFc variants was mixed well with an equal volume of 2.4 nM of myostatin or 2.4 nM of activin A at room temperature for 30 min. Upon complete aspiration of the growth medium from the white 96-well cell plate, 100 µl of the mixture was immediately added into individual wells of the plate. The cell plate was incubated for 20 h at 37°C. The next day, 100 ul/well of ONE-Glo luciferase assay system (Promega, Madison, WI) was directly added into individual wells of the cell plate, and the luminescence signal from the cell plate was measured in a FlexStation 3 instrument (Molecular Devices, Sunnyvale, CA). Induction of SMAD-responsive reporter (i.e., 100% signals) was produced by either 2.4 nM myostatin or 2.4 nM activin alone, and negative control (i.e., 0% signals) was produced by A204 assay medium alone. IC_{50} curves were fitted using Graphpad Prism software (GraphPad Software, Inc., La Jolla, CA).

Glycan Analysis. Protein samples were analyzed as described previously (Traylor et al., 2016) with a few differences. Samples were alkylated with iodoacetamide (ThermoFisher Scientific) and digested only with sequencing-grade endoprotease Lys-C (Roche Diagnostics, Switzerland). Analyses were performed with an Acquity Classic UPLC (Waters) with an inline QExactive Plus Orbitrap or an LTQ Orbitrap Velos mass spectrometer (ThermoFisher Scientific). Samples were separated on a CSH300 2.1 × 100 mm chromatography column with 1.7 μm particles (Waters).

Mass spectrometry data were analyzed with PepFinder 2.0 (ThermoFisher Scientific). A modification list was generated using the default software parameters and exported into Microsoft Excel. The identified glycan modifications were used to calculate sialic acid content in units of mole sialic acid per mole oligosaccharide. For each identified glycan modification, the percent abundance was multiplied by the number of sialic acid units on the oligosaccharide and divided by the glycan occupancy to normalize the calculation to the total quantity of oligosaccharide at the particular site. The sum of this quantity for all identified glycans at an N-linked site yields the sialic acid abundance in units of mole sialic per mole oligosaccharide. If an oligosaccharide is present (i.e., the site is occupied), the sialic acid content value provides the average quantity of sialic acid on the oligosaccharide. The percentage of asialylated oligosaccharide was calculated by adding all the percentage of the oligosaccharide species without terminal sialic acid together then dividing this value by the oligosaccharide occupancy at the particular glycosylation site. The percentage of different antennary (branch) structures was calculated similarly by adding the percentage of oligosaccharides with particular antennary structures (e.g., bi-, tri-, tetra-antennary) and then dividing that value by the oligosaccharide occupancy at the particular glycosylation site.

Polyacrylamide Gel Electrophoresis and Coomassie Blue Staining. 3 μg purified recombinant FS315-hFc protein sample was mixed with Bond-Breaker Tris(2-

carboxyethyl)phosphine hydrochloride solution (ThermoFisher Scientific) and NuPAGE LDS Sample Buffer (4x) (Life Technology), and then incubated at 37°C 15 min. The mix was run on a NuPAGE Novex 4-12 % gradient Bis-Tris gel (Life Technology) for 35 min at 190 V in NuPAGE Novex MES SDS Running Buffer (Life Technology). The Coomassie blue staining was carried out using InstantBlue (Expedeon, San Diego, CA) by following the instructions.

Murine Pharmacokinetic (PK) Studies. CD-1 female mice at 4-5 weeks of age were obtained from Charles River Laboratories (Wilmington, MA). Mice were housed in groups of 3 per cage under a 12 h light-dark cycle, targeted humidity (50% ± 20%) and temperature (22°C ± 3°C). Rodent diet (LabDiet-5001, St Louis, MO) and water (Lexington, MA, municipal water purified by reverse osmosis) was available ad libitum for the duration of the experiment. Care of animals was conducted in accordance with the guidelines described in the Guide for the Care and Use of Laboratory Animals (National Academy Press, Washington D.C., 2011). All *in vivo* procedures described were approved by Shire Pharmaceuticals Institutional Animal Care and Use Committee.

Animals were handled with aseptic technique and were placed in a restrainer for intravenous injection. The site was wiped with 70% ethanol and the tail vein was dilated by flicking the tail gently with the finger. All FS315-hFc variants, diluted in 1X PBS (pH 7.4), were injected into the vein using a 28 gauge insulin syringe to a final dosing volume of 1 mg/kg individually. At each time point, 3 animals were euthanized using carbon dioxide inhalation and cardiac puncture was used to collect a blood sample. Blood was added to a serum separator tube, centrifuged for 3 min at 13,200 rpm, and serum was collected in an Eppendorf tube and frozen at -80°C.

Immunoassays for the PK Samples and PK Data Analysis. Serum concentrations of FS315-hFc variants were determined using an electro-chemiluminescent immunoassay. Meso

Scale Discovery standard plates (MSD, Rockville, MD) were coated with 10.0 µg/ml goat anti-human Follistatin antibody (R&D Systems, AF669) in 1x PBS, 30 µl/well. After overnight incubation at 4°C, plates were washed 3 times with wash buffer (20% Tween-20 in 1x PBS) and then blocked with 150 µl/well blocking buffer (2.5% bovine serum albumin, 0.05% Casein in 1x PBS) and incubated at 25°C for 1 h with shaking. After washing 3 times with wash buffer, samples and a standard curve of FS315-hFc variants ranging from 0.98-125 ng/ml were added, 25 µl/well. Samples, controls and standards were incubated at 25°C for 1 h with shacking. After washing 3 times with wash buffer, 25 µl/well of 2.5 µg/ml mouse anti human IgG1-Fc (Abcam, Cambridge, MA) labeled using Gold Sulfo-Tag NHS Ester (MSD, R91AO) was added. After incubation at 25°C for 1 h with shaking, and washing 3 times with wash buffer, 1X Read Buffer T (MSD, R92TC) was added, 150 µl/well. Plates were read with a SECTOR imager (MSD) and concentrations determined relative to the standard curve, adjusted for dilutions.

Non-compartmental pharmacokinetic analysis of serum concentration data of FS315-hFc variants was performed using Phoenix WinNonlin (Version 6.3, Pharsight Corporation, Mountain View, CA). Pharmacokinetic parameters such as systemic T½ (terminal half-life, which was determined using the last 4 time points), CL (clearance), V_{ss} (steady state volume of distribution), and AUC (area under the curve) were calculated.

Results

The Charge of the Basic BBXB Motifs within the FS HBS Affects the Heparin Binding Affinity. Rapid heparin-mediated hepatic clearance of native FS, even when fused to the antibody Fc fragment, limits its therapeutic potential as shown from published data (Datta-Mannan et al., 2013) and our unpublished data (data not shown). To overcome this limitation, we targeted the heparin binding loop of FS for modulating heparin binding activity by site-directed mutagenesis. Sidis et al (Sidis et al., 2005) previously showed that the mutations of lysine (K) residues within the FS288 isoform heparin binding motifs ((K(75,76)A, K(81,82)A and K(76,81,82)A)) resulted in decreased heparin binding in a competition assay. We firstly hypothesized that substitution of positive charged residues within two BBXB motifs with amino acids having a negative charge will result in an even greater heparin binding decrease than seen with alanine (A) substitutions. To test this hypothesis, we generated K(81,82)E, K(81,82)D, K(76,81,82)E and K(76,81,82)D variants to compare with K(81,82)A and K(76,81,82)A. Because of the poor expression of FS288 in our study, which was also reported by others (Datta-Mannan et al., 2013), all the variants were recombinant proteins of the FS315 isoform fused to human IgG1 Fc (FS315-hFc) directly. The protein sequence of hFc region used in this study is shown in supplemental data. The binding interaction between FS315-hFc variants and heparin was measured using SPR method. The binding affinities were measured and reported by the equilibrium dissociation constant (K_D) (Table 1 and Supplemental Table 3). After substitution to more negative residues, both K(81,82)E and K(81,82)D had >7-fold reduction in heparin binding compared to K(81,82)A, indicating the further impaired heparin binding activity. Consistently, the triplet variants K(76,81,82)E and K(76,81,82)D also had highly reduced affinities compared to K(76,81,82)A. Molecules containing both E and D triplet variants had no detectable heparin binding in our testing range (up to 25 nM). However, the heparin SPR binding K_D was 9.4 nM for K(76,81,82)A, having either comparable or even stronger affinity than the doublet K(81,82)E and K(81,82)D variants. This data support our

hypothesis that changing the charge of the basic BBXB motifs within the FS HBS significantly affects the binding affinity to heparin.

Extent and Position of Glutamic Acid (E) Substitutions in Two Basic BBXB Motifs Affect the Heparin Binding Affinity. Our above data also suggested that the triplet K(76,81,82)E and K(76,81,82)D variants which altered two BBXB motifs showed greater reduction on affinities compared with doublet K(81,82)E and K(81,82)D variants which only altered one of the two BBXB motifs, indicating that both motifs contribute to the heparin binding (Table 1). To further understand the role of the key basic residue(s) within the two BBXB motifs on the heparin binding affinity, we generated a series of FS315-hFc variants in which we replaced one, two or three basic residues(s) with negatively charged E within BBXB motifs. We also generated two recombinant heparin-binding deficient variants with larger changes: 1) FS315ΔHBS-hFc, a HBS replacement variant ΔHBS in which the HBS (residues 75-86) was replaced by the corresponding segment from FSD2 (residues 148-159) that lacks any heparin binding capability as described by Sidis et al.(Sidis et al., 2005), and 2) FS315del75-86-hFc, a HBS deletion variant del75-86 in which the core 12 amino acid HBS was deleted. The recombinant wild type FS315 isoform fused with hFc, which had similar potency to myostatin and activin as native FS315 (R&D Systems, cat#4889-FN/CF) in our cell-based assay (unpublished data), was named as "wild type" and used as the control in this paper. The HBS sequences for wild type and all heparin-binding variants are listed in Supplemental Table 1. The SPR binding data showed that all of the variants with one, two or three E substitutions had reduced heparin affinities to different degrees compared with wild type (4~100-fold reduction or undetectable binding in our testing range) (Table 1). In general, increasing the extent of E substitutions progressively decreased the heparin binding. For example, the heparin binding K_D values were 1.5 nM, 10.7 nM and undetectable binding in the tested range for K82E, K(81,82)E and K(76,81,82)E variants, respectively. K(76,81,82)E, ΔHBS, and del75-86 variants all

showed similar abolished heparin binding (Table 1), indicating that FS heparin binding affinities can be effectively abolished with three negative charged point mutations.

By systematically evaluating the different variants, additional two conclusions can be drawn about the role of basic residues in two FS BBXB motifs. Firstly, the second BBXB motif KKNK (residues 81-84) clearly plays a more dominant role in heparin binding than the first BBXB motif KKCR (residues 75-78), as indicated by K(81,82)E (K_D 10.7nM) having ~10-fold weaker binding compared to K(75,76)E (K_D 1.1 nM) (Table 1). Secondly, the third basic residue in each of FS BBXB motifs has much less effect on heparin binding. Our data (Table 1) showed that: 1) a doublet variant K(76,82)E with the second basic residues mutations in both motifs had 5 fold weaker binding than a doublet variant R78E/K84E with the third basic residues mutations in both motifs; 2) adding mutations of the third basic residue from each motifs (R78E and K84E) to K82E variant did not affect the binding affinity, as the K_D values for K82E, R78E/K82E, and K(82,84)E were 1.5 nM, 1.3 nM and 1.1 nM, respectively;   and 3) K(81,82)E variant binds to heparin ~10-fold weaker than K(82,84)E variant, 10.7 nM vs. 1.1 nM; and K(76,81,82)E had much weaker binding affinity than K(76,82,84)E as well, indicating a minor role of K84. All the data demonstrated that the first two basic residues are more important than the third basic residue in FS BBXB motifs for heparin binding. Taken together, our data above demonstrate that the number of mutations and their positions, and the charge of the residue affect the heparin binding affinity.

In Vitro Ligand Binding and Functional Properties for Heparin Binding Variants.
Contrast to the large differences observed for heparin binding affinities among FS315-hFc variants substituted with negatively charged amino acids (4 to >100-fold reduction compared to wild type), the variants exhibited little changes in binding affinity to myostatin. The K_D values determined by the SPR method are summarized in Table 1. Uniquely, several of the heparin binding variants had moderately improved myostatin binding affinities by SPR assay (1.5 to 5-

fold increase compared with wild type). The HBS deletion variant del75-86 performed differently, which showed a 3-fold reduction compared to wild type. To test if the variants change FS biological function, we selected a subset of variants, and tested their inhibition of myostatin- and activin A- induced SMAD signaling using a SMAD-responsive luciferase reporter assay in A204 rhabdomyosarcoma cells. For all heparin binding variants with the one, two or three point mutation(s), potencies of inhibiting myostatin signaling or activin signaling were similar, and comparable to wild type (Table 2 and Fig. 2A). The HBS deletion (del75-86) variant showed more than 10-fold reduction in both myostatin inhibition and activin inhibition compared to wild type in the cell-based assay (Table 2). The weaker affinity between the del75-86 variant and its ligands caused unsaturated and extended IC_{50} curves (Figure 2A). However, we did not see any functional reduction for the HBS replacement variant ΔHBS (Table 2), suggesting that the deletion of amino acids 75-86 may change the conformation of the molecule.

We also tested if the mutations in the BBXB motifs affect the interaction between the hFc portion of our recombinant variants and hFcRn by SPR under acidic condition. With the mutations located in the HBS region in FSD1 and the hFc portion fused to C-terminus, there were no obvious affinity changes to hFcRn for our heparin binding variants compared to wild type (Table 1). The pI values for most of our variants with the negatively charged amino acids substitutions, as well as for the ΔHBS and del75-86 variants, were clearly shifted to the acidic range (Table 1).

Binding Affinity to Heparin Affects *In Vivo* PK Profile. As described above, by rational mutagenesis of the basic BBXB motifs, we were able to generate a series of variants with different *in vitro* heparin binding affinities. Heparin binding is a surrogate for the association with cell surface heparan sulfate proteoglycans, which is a critical process for internalization and clearance for many proteins *in vivo* (Bernfield et al., 1999). We were interested to investigate the effect of modulated heparin binding affinity on PK profile in mice. Selected HBS variants

with different heparin binding affinities were administered as single intravenous doses (1 mg/kg) to female CD1 mice. The serum exposures of these molecules were monitored up to 168 h post dosing. Following a single 1 mg/kg i.v. dose, wild type had a clearance rate and half-life of 30 ml/h/kg and 68 h, respectively, and the ΔHBS variant had a much lower clearance and longer half-life of 1.3 ml/h/kg and 92 h, respectively (Table 3), consistent with previously published data (Datta-Mannan et al., 2013). All of tested newly designed heparin binding variants showed improved PK profiles compared to the wild type (Fig. 3 and Table 3). Strikingly, we observed a clear correlation between the degree of heparin binding affinity *in vitro* and the exposure measured as Area Under the Curve (AUC) *in vivo*. Diminishing *in vitro* heparin binding affinity correlated to progressively increased AUC (Fig. 3A) and progressively decreased clearance (Fig. 3B) compared to wild type, ranging from 2 ~ 25-fold shift for tested variants. The steady state volumes of distribution (V_{ss}) were highly decreased for the heparin binding variants compared to wild type (Table 3), indicating that reducing heparin binding affinity had a significant impact on apparent volume of distribution, which should be mainly caused by decreased association with cell surface heparan sulfate proteoglycans. The data above clearly demonstrate the critical impact of the heparin binding on the *in vivo* PK properties.

Datta-Mannan et al. previously reported that a recombinant FS heparin-binding deficient mutant, with a paralogous substitution to remove the heparin-binding loop, had ~8-fold and ~3-fold improved AUC and half-life respectively compared to the recombinant wild type FS in mice (Datta-Mannan et al., 2013). In our studies, variant K(76,81,82)E with no measurable heparin binding had ~20-fold improved AUC and ~2-fold improved half-life compared to the recombinant wild type, and even had moderate improved AUC and half-life compared to ΔHBS variant in mice (Table 3). In addition, K(76,81,82)E also showed better developability properties compared to the ΔHBS variant in our studies, including increased protein expression and reduced aggregation (data not shown). Based on the improved PK profile and developability characteristics described here, the recombinant K(76,81,82)E variants (fused with either human

Fc or murine Fc) were used for pharmacodynamics studies, and resulted in significantly increased muscle mass and functional improvement in a dose-dependent manner (manuscript in preparation, Shire).

Novel N-linked Glycosylation Consensus Sequences Introduced for Hyperglycosylation. In our study, we also used a more surgical approach to the mutagenesis described above to generate potentially hyperglycosylated recombinant FS315-hFc variants by introducing new N-linked glycosylation consensus sequences into the heparin-binding loop. Our rationale for this approach included reducing immunogenicity risk, modulating the carbohydrate content to decrease clearance, and blocking heparin binding by adding a negatively charged, bulky glycan structure. We designed 10 new variants representing 6 consensus N-linked glycosylation sites, NXT/S, where X can be any amino acid except proline, on positions 74, 75, 78, 80, 83 and 86 within the HBS region (sequences are listed in Supplemental Table 2). Initial detection of incorporation of additional carbohydrate moiety was observed by the molecular weight shift on sodium dodecyl sulfate polyacrylamide gel electrophoresis. Compared to wild type and other variants, variant K75N/C77T/K82T showed a clear shift to a higher molecular weight (Fig. 4A), suggesting incorporation of a glycan. Two additional variants (C66A/K75N/C77T and C66S/K75N/C77T) showed a less pronounced shift to a higher molecular weight (Fig. 4A). All three of these variants have the common mutated sites K75N/C77T. cIEF data showed that the K75N/C77T/K82T variant had a clear acidic shift of pI compared to a K82T variant (Fig. 4B), indicating the potential occupation of a negatively charged glycan moiety at the N75 site causing both the molecular weight and pI shift. To further confirm the status of the glycan occupation on all introduced N-linked glycosylation sites, we did chromatography and mass spectrometry-based characterization. Mass spectrometry data confirmed that, among six sites we studied in the heparin-binding loop, we were able to generate hyperglycosylated FS by introducing a glycosylation consensus site on position 75

18

(Table 4). The three variants K75N/C77T/K82T, C66A/K75N/C77T, and C66S/K75N/C77T containing the same K75N/C77T mutations had variable glycan occupancy (69.7%, 39.6%, and 21.5%) with similar mole sialic acid per mole oligosaccharide ratios (1.99, 1.88, and 1.96) on N75 (Table 4). Despite the occupancy difference, the major oligosaccharide species were similar on N75 as well as the three native N-linked sites, including high levels of bi-antennary, tri-antennary and tetra-antennary structures, and low levels of high mannose structures (Supplemental Fig. 1). Although the levels of asialylated oligosaccharide at all N-linked sites were comparable for the three hyperglycosylated variants, in general, K75N/C77T/K82T had overall higher occupancy and lower asialylated percentage than the other hyperglycosylated variants (Table 4 and Supplemental Fig. 2). The overall higher glycosylation occupancy on K75N/C77T/K82T was consistent with its greater mobility shift on polyacrylamide electrophoresis gel (Fig. 4A).

In Vitro Binding Characteristics and In Vivo PK Properties of the Hyperglycosylation Variants. One rationale of designing new hyperglycosylation sites within the HBS region was in an attempt to block heparin binding by introducing negatively charged and bulky glycan structures. For the three hyperglycosylated variants with glycan occupation on N75, *in vitro* heparin binding affinity reduction (~15-fold reduction compared with wild type) was only observed with variant K75N/C77T/K82T, which had the highest glycan occupancy on N75, as well as a K82T mutation in the second BBXB motif (Table 5 and Supplemental Table 4), indicating that the effect of glycan on N75 on heparin binding activity could be moderate. The three hyperglycosylated variants showed slight or moderate myostatin binding reduction compared to wild type as measured by SPR (Table 5 and Supplemental Table 4). In the A204 cell-based reporter assay, the three hyperglycosylated variants had 2 to 3-fold reduction in myostatin inhibition and 2 to 4-fold reduction in activin A inhibition compared to wild type and

19

other non-hyperglycosylated variants (Table 2 and Fig. 2B), indicating a slight inhibition of potency by the additional glycan.

To determine the effect of hyperglycosylation on PK profiles, we performed mouse PK studies using selected molecules, including non-hyperglycosylated variant K82T, two hyperglycosylated variants K75N/C77T/K82T and C66A/K75N/C77T, as well as wild type and ΔHBS as controls. K82T, K75N/C77T/K82T and C66A/K75N/C77T were selected for the mouse PK study due to the similarities in glycan structure and distribution, the level of high mannose structure, and the percentage of asialyted structure on the three native N-linked sites for these variants (Table 4, Supplemental Fig. 1 and Supplemental Fig. 2), which enabled us to assess the effect of glycosylation state on the PK profile primarily from the newly introduced N-linked site. Our data show that the non-hyperglycosylated variant K82T had similar but slightly improved PK characteristics compared to wild type. However, the two hyperglycosylated variants had significantly improved PK profiles compared to K82T and wild type (Fig. 5 and Table 3). Variant C66A/K75N/C77T showed 6 ~ 10-fold higher exposure, and variant K75N/C77T/K82T showed 10 ~ 17-fold higher exposure compared to K82T and wild type, which was similar to the heparin binding deficient variant ΔHBS (Fig. 5 and Table 3). The significant difference between the hyperglycosylated variants and the non-hyperglycosylated variant indicate that the increased carbohydrate content directly modulates PK parameters. The K75N/C77T/K82T variant had the highest glycosylation content and sialic acid percentage, as well as weaker heparin binding, which could explain its greater improvement on PK profile than C66A/K75N/C77T. Our data above indicate that modulating heparin binding activity and glycosylation content could be attractive approaches to improve PK properties of FS fusion proteins.

Discussion

A number of studies have investigated the importance of FS domains and residues on its biological activities by chemical modifications and mutational analyses (Harrison et al., 2006; Keutmann et al., 2004; Sidis et al., 2005; Zheng et al., 2017). However, systematical protein engineering of recombinant FS for therapeutic applications is largely unexplored. Recently, a recombinant human FS315 variant with the replacement of the HBS region and fused with murine IgG1 Fc has been shown to greatly extend the exposure and half-life *in vivo*, conferring skeletal muscle hypertrophy and improvement in mouse tissue repair after injury (Datta-Mannan et al., 2013; Yaden et al., 2014). In our study, to further understand the impact that heparin binding affinity on molecular properties and pharmacokinetic behavior, we have systematically engineered a series of recombinant FS315 variants fused to human IgG1 Fc by site-directed mutagenesis.

In this study, we demonstrated that the charge of key residues in the basic BBXB motifs within the FS HBS significantly affects the heparin binding affinity. FS315 is composed of an N-terminal domain, three FS domains (FSD1, FSD2 and FSD3), and a highly acidic C-terminal tail (Fig. 1). Two core heparin-binding motifs KKCR and KKNK that are rich in basic residues are located in the FSD1, which makes it the most basic domain (pI 8.9) compared with FSD2 (pI 6.7) and FSD3 (pI 4.8) (Innis and Hyvonen, 2003). Structural analysis of 20 non-redundant three-dimensional protein structures in complex with heparin showed that electrostatic and hydrogen-bonding interactions contribute the most in the binding between cationic residues (K or R) and anionic groups in heparin (Torrent et al., 2012). A crystal structure of the FS FSD1 domain complexed with heparin analogs also indicated that heparin analogs associate with the highly basic HBS through their negatively charged sulfate groups by electrostatic interactions (Innis and Hyvonen, 2003). We hypothesized that substituting cationic residues with anionic residues in the BBXB motifs of the HBS region will break the electrostatic interactions and abolish heparin binding. Indeed, our negative-residue substituted variants K(76,81,82)E and

K(76,81,82)D had undetectable heparin binding affinities in SPR binding assays, whereas a neutral-residue substituted variant K(76,81,82)A had a binding K_D of 9.4nM, confirming the greater effect on eliminating heparin binding using negatively charged substitutions. With the significant impact of negative charged substitutions on heparin binding affinity, we were able to make only a few point mutations to achieve the same change in binding as seen with the HBS replacement variant ΔHBS and the HBS deletion variant del75-86 (Table 1). In our hands, utilizing minimal substitutions allowed for improved expression levels for our FS variants in CHO cells and reduced protein aggregation in our protein A eluate, as well as retained similar activin A and myostatin binding affinities as wild type.

By generating a series of one, two, or three amino acid substitutions for the key residues in the BBXB motifs using the negatively charged residue glutamic acid E, we were able to: 1) identify the key positions and combinations for heparin binding. Our screening of six basic residues in the two BBXB motifs indicated that K81 and K82 in the second BBXB motif play a dominant role for the electrostatic interaction since we observed the highest impact on heparin binding with the doublet variant K(81,82)E compared to six other doublet variants, including K(75,76)E, K(76,82)E, K(76,84)E, R78E/K82E, R78E/K84E and K(82,84)E (Table 1). Interestingly, we also found that variants with the K82E mutation consistently showed a ~2-fold increase in protein expression levels (data not shown), implying the positive impact of K82E on protein folding; 2) generate variants with different degrees of heparin binding, having a range of 4 to >100-fold reduction in our testing range compared to wild type. It has been shown that the association between FS and cell-surface heparan sulfate proteoglycans caused rapid cellular uptake and clearance (Hashimoto et al., 1997). Since it was of interest to us how the different degree of *in vitro* heparin binding correlated to *in vivo* PK profiles, we selected multiple variants with different heparin binding affinities, and administered them as a single intravenous doses (1 mg/kg) to female CD1 mice. All of the variants showed improved PK profiles compared to wild type, and more strikingly, decreased heparin-binding clearly correlated with increased AUC and

decreased clearance (Fig. 3 and Table 3). The significantly decreased apparent volumes of distribution for heparin binding variants, which were reflected in V_{ss} (Table 3), strongly support that the association with cell surface heparan sulfate proteoglycans is one of the determinant processes for the *in vivo* PK profile of follistatin protein. In contrast to the clear relationship between heparin binding affinity and either AUC or clearance, we did not see this direct relationship on the terminal half-life. Compared with the significant impact of heparin binding affinity on the distribution phase, the terminal half-life was mainly driven by elimination pathways, such as FcRn-dependent interaction for recombinant Fc-fusion proteins; 3) retain unchanged ligand binding potency compared to wild type (Table 2 and Fig. 2A), which supports published studies that both N-terminal domain and FSD2 may be the essential determinants for either myostatin or activin binding (Keutmann et al., 2004; Zheng et al., 2017).

Our heparin binding variants with introduced negative residues have lower pI values than wild type. Published work demonstrated that an antibody with a lower pI had a longer half-life, proposed to be due to a decreased amount of fluid phase pinocytosis (Igawa et al., 2010; Li et al., 2014). This is consistent with our negatively charged heparin binding variants having reduced association with cell-surface heparan sulfate proteoglycans, therefore having a reduced cellular uptake and clearance.

Glycoengineering technology is becoming an attractive strategy to improve the pharmaceutical properties of therapeutics. There are many approaches for glycoengineering, including the introduction of new glycosylation sites to increase carbohydrate content or to block specific binding (Mimura et al., 2017; Yu et al., 2017). In this study, we generated 10 variants with six new consensus N-linked glycosylation sites within the HBS region. Among the designed six positions, we were able to identify a hyperglycosylation site on N75 (Table 4). The crystal structure of FSD1 indicates that residues 64-74 form a loop, followed by strand β1 (residues 75-79) and strand β2 (residues 85-89). Residue 75 locates in a type II β-turn (residues 72-75) which connects the loop and strand β1 (Innis and Hyvonen, 2003), consistent with the

finding that glycosylation is often occurring at an exposed loop region with some flexibility (Samoudi et al., 2015). Interestingly, not much glycan occupancy was observed on the neighboring site N74 (Table 4), suggesting the potential importance of three-dimensional structures on glycosylation.

Glycosylation is the most complex post-translational process. During the production process various parameters impact glycan structures, including cell culture conditions, protein structure and protein folding. Methods to modulate glycosylation heterogeneity for glycoproteins in mammalian cell culture have been well documented during the manufacturing process, including optimizing pH, temperature, oxygen concentration, the medium formulation and feed rate, expression level, and production method (batch, fed-batch, perfusion) (Hossler, 2012). In our study, we used consistent expression and culture conditions for our variants to reduce glycosylation heterogeneity caused by culture environment. We observed consistent high occupancy on N259, however, both N95 and N112 were variably occupied for different FS315-hFc variants (Table 4). Although varied in occupancy, the major glycan species and their abundances at each N-linked site was similar for different FS315-hFc variants (Supplemental Fig. 1 and data not shown). For example, at N95, the most abundant glycan species were tetra-antennary, tri-antennary, and bi-antennary complex oligosaccharides with sialic acids fully or partially occupied at the terminal (Supplemental Fig. 2). For simplification, the sialic acid content was chosen to evaluate the overall terminal sialic acid level in different variants in this study. It has been reported that poorly sialylated recombinant FS proteins had a quicker clearance because of asialoglycoprotein receptor-mediated clearance (Datta-Mannan et al., 2015). Two hyperglycosylated variants K75N/C77N/K82T and C66A/K75N/C77T showed significantly improved *in vivo* exposure compared to wild type and non-hyperglycosylated variant K82T in mouse studies (Fig. 5), indicating that the glycan occupancy on new introduced N-linked site may have increased sialic acid content, and could block some heparin-binding by addition of a bulky glycan *in vivo*. Our data suggest that the addition of a hyperglycosylation

modification could be a surgical approach to the HBS variants to achieve further improved PK properties and reduce the immunogenicity risk.

In summary, the data collected from our engineered FS315-hFc recombinant variants focused on the manipulation of heparin-binding affinity, and the evaluation of the impact of the mutations on PK properties. This comprehensive study provides valuable information for potential pharmacologic application of improved recombinant FS molecules. Certain selected variants, such as K(76,81,82)E, showed promising pharmacodynamics in pharmacology studies (manuscript in preparation, Shire). Manipulating heparin-binding activity, glycosylation content, and/or the myostatin binding affinity by protein engineering could be attractive strategies for generating novel molecules with desirable therapeutic properties. Further studies should be considered to explore a clear exposure-response relationship for these novel variants in the content of different therapeutic applications.

Acknowledgments

Authorship Contributions

Participated in research design: Norton, Iskenderian, Pan, Shen, Meiyappan, Zhang, Gill

Conducted experiments: Shen, Iskenderian, Lundberg, He, Palmieri, Crooker, Deng, Traylor,

Gu, Pescatore, Strack-Logue, Romashko, Baviello

Performed data analyses: Rong, Palmieri, Crooker, Traylor

Wrote or contributed to the writing of the manuscript: Shen, Iskenderian, Norton, Pan, Ehmann,

Lundberg, He, Palmieri, Deng, Traylor, Rong, Zhang, Meiyappan

References

Bernfield M, Gotte M, Park PW, Reizes O, Fitzgerald ML, Lincecum J and Zako M (1999) Functions of cell surface heparan sulfate proteoglycans. *Annu Rev Biochem* **68**:729-777.

Cash JN, Angerman EB, Keutmann HT and Thompson TB (2012) Characterization of follistatin-type domains and their contribution to myostatin and activin A antagonism. *Mol Endocrinol* **26**:1167-1178.

Chen PR and Lee K (2016) INVITED REVIEW: Inhibitors of myostatin as methods of enhancing muscle growth and development. *J Anim Sci* **94**:3125-3134.

Datta-Mannan A, Huang L, Pereira J, Yaden B, Korytko A and Croy JE (2015) Insights into the Impact of Heterogeneous Glycosylation on the Pharmacokinetic Behavior of Follistatin-Fc-Based Biotherapeutics. *Drug Metab Dispos* **43**:1882-1890.

Datta-Mannan A, Yaden B, Krishnan V, Jones BE and Croy JE (2013) An engineered human follistatin variant: insights into the pharmacokinetic and pharmocodynamic relationships of a novel molecule with broad therapeutic potential. *J Pharmacol Exp Ther* **344**:616-623.

Dennler S, Itoh S, Vivien D, ten Dijke P, Huet S and Gauthier JM (1998) Direct binding of Smad3 and Smad4 to critical TGF beta-inducible elements in the promoter of human plasminogen activator inhibitor-type 1 gene. *EMBO J* **17**:3091-3100.

Esch FS, Shimasaki S, Mercado M, Cooksey K, Ling N, Ying S, Ueno N and Guillemin R (1987) Structural characterization of follistatin: a novel follicle-stimulating hormone release-inhibiting polypeptide from the gonad. *Mol Endocrinol* **1**:849-855.

Haidet AM, Rizo L, Handy C, Umapathi P, Eagle A, Shilling C, Boue D, Martin PT, Sahenk Z, Mendell JR and Kaspar BK (2008) Long-term enhancement of skeletal muscle mass and strength by single gene administration of myostatin inhibitors. *Proc Natl Acad Sci U S A* **105**:4318-4322.

Harrison CA, Chan KL and Robertson DM (2006) Activin-A binds follistatin and type II receptors through overlapping binding sites: generation of mutants with isolated binding activities. *Endocrinology* **147**:2744-2753.

Hashimoto O, Nakamura T, Shoji H, Shimasaki S, Hayashi Y and Sugino H (1997) A novel role of follistatin, an activin-binding protein, in the inhibition of activin action in rat pituitary cells. Endocytotic degradation of activin and its acceleration by follistatin associated with cell-surface heparan sulfate. *J Biol Chem* **272**:13835-13842.

Hossler P (2012) Protein glycosylation control in mammalian cell culture: past precedents and contemporary prospects. *Adv Biochem Eng Biotechnol* **127**:187-219.

Igawa T, Tsunoda H, Tachibana T, Maeda A, Mimoto F, Moriyama C, Nanami M, Sekimori Y, Nabuchi Y, Aso Y and Hattori K (2010) Reduced elimination of IgG antibodies by engineering the variable region. *Protein Eng Des Sel* **23**:385-392.

Innis CA and Hyvonen M (2003) Crystal structures of the heparan sulfate-binding domain of follistatin. Insights into ligand binding. *J Biol Chem* **278**:39969-39977.

Inouye S, Ling N and Shimasaki S (1992) Localization of the heparin binding site of follistatin. *Mol Cell Endocrinol* **90**:1-6.

Jefferis R (2016) Glyco-Engineering of Human IgG-Fc to Modulate Biologic Activities. *Curr Pharm Biotechnol* **17**:1333-1347.

Keutmann HT, Schneyer AL and Sidis Y (2004) The role of follistatin domains in follistatin biological action. *Mol Endocrinol* **18**:228-240.

Kota J, Handy CR, Haidet AM, Montgomery CL, Eagle A, Rodino-Klapac LR, Tucker D, Shilling CJ, Therlfall WR, Walker CM, Weisbrode SE, Janssen PM, Clark KR, Sahenk Z, Mendell JR and Kaspar BK (2009) Follistatin gene delivery enhances muscle growth and strength in nonhuman primates. *Sci Transl Med* **1**:6ra15.

Lalonde ME and Durocher Y (2017) Therapeutic glycoprotein production in mammalian cells. *J Biotechnol* **251**:128-140.

Latres E, Pangilinan J, Miloscio L, Bauerlein R, Na E, Potocky TB, Huang Y, Eckersdorff M,
Rafique A, Mastaitis J, Lin C, Murphy AJ, Yancopoulos GD, Gromada J and Stitt T
(2015) Myostatin blockade with a fully human monoclonal antibody induces muscle
hypertrophy and reverses muscle atrophy in young and aged mice. *Skelet Muscle* **5**:34.

Lee SJ, Reed LA, Davies MV, Girgenrath S, Goad ME, Tomkinson KN, Wright JF, Barker C,
Ehrmantraut G, Holmstrom J, Trowell B, Gertz B, Jiang MS, Sebald SM, Matzuk M, Li E,
Liang LF, Quattlebaum E, Stotish RL and Wolfman NM (2005) Regulation of muscle
growth by multiple ligands signaling through activin type II receptors. *Proc Natl Acad Sci
U S A* **102**:18117-18122.

Li B, Tesar D, Boswell CA, Cahaya HS, Wong A, Zhang J, Meng YG, Eigenbrot C, Pantua H,
Diao J, Kapadia SB, Deng R and Kelley RF (2014) Framework selection can influence
pharmacokinetics of a humanized therapeutic antibody through differences in molecule
charge. *MAbs* **6**:1255-1264.

Mendell JR, Sahenk Z, Al-Zaidy S, Rodino-Klapac LR, Lowes LP, Alfano LN, Berry K, Miller N,
Yalvac M, Dvorchik I, Moore-Clingenpeel M, Flanigan KM, Church K, Shontz K, Curry C,
Lewis S, McColly M, Hogan MJ and Kaspar BK (2017) Follistatin Gene Therapy for
Sporadic Inclusion Body Myositis Improves Functional Outcomes. *Mol Ther* **25**:870-879.

Mendell JR, Sahenk Z, Malik V, Gomez AM, Flanigan KM, Lowes LP, Alfano LN, Berry K,
Meadows E, Lewis S, Braun L, Shontz K, Rouhana M, Clark KR, Rosales XQ, Al-Zaidy
S, Govoni A, Rodino-Klapac LR, Hogan MJ and Kaspar BK (2015) A phase 1/2a
follistatin gene therapy trial for becker muscular dystrophy. *Mol Ther* **23**:192-201.

Mimura Y, Katoh T, Saldova R, O'Flaherty R, Izumi T, Mimura-Kimura Y, Utsunomiya T,
Mizukami Y, Yamamoto K, Matsumoto T and Rudd PM (2017) Glycosylation engineering
of therapeutic IgG antibodies: challenges for the safety, functionality and efficacy.
Protein Cell.

Nakamura T, Sugino K, Titani K and Sugino H (1991) Follistatin, an activin-binding protein, associates with heparan sulfate chains of proteoglycans on follicular granulosa cells. *J Biol Chem* **266**:19432-19437.

Namwanje M and Brown CW (2016) Activins and Inhibins: Roles in Development, Physiology, and Disease. *Cold Spring Harb Perspect Biol* **8**.

Robertson DM, Klein R, de Vos FL, McLachlan RI, Wettenhall RE, Hearn MT, Burger HG and de Kretser DM (1987) The isolation of polypeptides with FSH suppressing activity from bovine follicular fluid which are structurally different to inhibin. *Biochem Biophys Res Commun* **149**:744-749.

Rodino-Klapac LR, Haidet AM, Kota J, Handy C, Kaspar BK and Mendell JR (2009) Inhibition of myostatin with emphasis on follistatin as a therapy for muscle disease. *Muscle Nerve* **39**:283-296.

Sako D, Grinberg AV, Liu J, Davies MV, Castonguay R, Maniatis S, Andreucci AJ, Pobre EG, Tomkinson KN, Monnell TE, Ucran JA, Martinez-Hackert E, Pearsall RS, Underwood KW, Seehra J and Kumar R (2010) Characterization of the ligand binding functionality of the extracellular domain of activin receptor type IIb. *J Biol Chem* **285**:21037-21048.

Samoudi M, Tabandeh F, Minuchehr Z, Ahangari Cohan R, Nouri Inanlou D, Khodabandeh M and Sabery Anvar M (2015) Rational design of hyper-glycosylated interferon beta analogs: a computational strategy for glycoengineering. *J Mol Graph Model* **56**:31-42.

Schneyer AL, Wang Q, Sidis Y and Sluss PM (2004) Differential distribution of follistatin isoforms: application of a new FS315-specific immunoassay. *J Clin Endocrinol Metab* **89**:5067-5075.

Schuelke M, Wagner KR, Stolz LE, Hubner C, Riebel T, Komen W, Braun T, Tobin JF and Lee SJ (2004) Myostatin mutation associated with gross muscle hypertrophy in a child. *N Engl J Med* **350**:2682-2688.

Shimasaki S, Koga M, Esch F, Cooksey K, Mercado M, Koba A, Ueno N, Ying SY, Ling N and Guillemin R (1988) Primary structure of the human follistatin precursor and its genomic organization. *Proc Natl Acad Sci U S A* **85**:4218-4222.

Sidis Y, Mukherjee A, Keutmann H, Delbaere A, Sadatsuki M and Schneyer A (2006) Biological activity of follistatin isoforms and follistatin-like-3 is dependent on differential cell surface binding and specificity for activin, myostatin, and bone morphogenetic proteins. *Endocrinology* **147**:3586-3597.

Sidis Y, Schneyer AL and Keutmann HT (2005) Heparin and activin-binding determinants in follistatin and FSTL3. *Endocrinology* **146**:130-136.

St Andre M, Johnson M, Bansal PN, Wellen J, Robertson A, Opsahl A, Burch PM, Bialek P, Morris C and Owens J (2017) A mouse anti-myostatin antibody increases muscle mass and improves muscle strength and contractility in the mdx mouse model of Duchenne muscular dystrophy and its humanized equivalent, domagrozumab (PF-06252616), increases muscle volume in cynomolgus monkeys. *Skelet Muscle* **7**:25.

Sugino K, Kurosawa N, Nakamura T, Takio K, Shimasaki S, Ling N, Titani K and Sugino H (1993) Molecular heterogeneity of follistatin, an activin-binding protein. Higher affinity of the carboxyl-terminal truncated forms for heparan sulfate proteoglycans on the ovarian granulosa cell. *J Biol Chem* **268**:15579-15587.

Torrent M, Nogues MV, Andreu D and Boix E (2012) The "CPC clip motif": a conserved structural signature for heparin-binding proteins. *PLoS One* **7**:e42692.

Traylor MJ, Tchoudakova AV, Lundquist AM, Gill JE, Boldog FL and Tangarone BS (2016) Comprehensive Discovery and Quantitation of Protein Heterogeneity via LC-MS/MS Peptide Mapping for Clone Selection of a Therapeutic Protein. *Anal Chem* **88**:9309-9317.

Ueno N, Ling N, Ying SY, Esch F, Shimasaki S and Guillemin R (1987) Isolation and partial
characterization of follistatin: a single-chain Mr 35,000 monomeric protein that inhibits
the release of follicle-stimulating hormone. *Proc Natl Acad Sci U S A* **84**:8282-8286.

Walton KL, Johnson KE and Harrison CA (2017) Targeting TGF-beta Mediated SMAD Signaling
for the Prevention of Fibrosis. *Front Pharmacol* **8**:461.

Welt C, Sidis Y, Keutmann H and Schneyer A (2002) Activins, inhibins, and follistatins: from
endocrinology to signaling. A paradigm for the new millennium. *Exp Biol Med (Maywood)*
227:724-752.

Yaden BC, Croy JE, Wang Y, Wilson JM, Datta-Mannan A, Shetler P, Milner A, Bryant HU,
Andrews J, Dai G and Krishnan V (2014) Follistatin: a novel therapeutic for the
improvement of muscle regeneration. *J Pharmacol Exp Ther* **349**:355-371.

Yu X, Marshall MJE, Cragg MS and Crispin M (2017) Improving Antibody-Based Cancer
Therapeutics Through Glycan Engineering. *BioDrugs* **31**:151-166.

Zheng H, Qiao C, Tang R, Li J, Bulaklak K, Huang Z, Zhao C, Dai Y, Li J and Xiao X (2017)
Follistatin N terminus differentially regulates muscle size and fat in vivo. *Exp Mol Med*
49:e377.

Legends for Figures

Figure 1. Protein Domain Structure of FS315. FS315 is comprised of an N-terminal domain (ND), three successive FS domains with high homology (FSD1, FSD2 and FSD3), and a highly acidic C-terminal tail (AD). The heparin-binding sequence (HBS) is located in the FSD1, and two conserved basic heparin-binding core motifs are shown in bold. The positions of three endogenous N-linked glycosylation sites are indicated by solid triangles.

Figure 2. *In Vitro* Cell-based Functional Assay. The inhibition to myostatin and activin A was investigated using a SMAD-responsive luciferase reporter assay in A204 rhabdomyosarcoma cells. (A) IC50 curves of myostatin and activin A for representative FS315-hFc heparin binding variants. Single, double and triple mutations had no effect on functional activities, but the HBS del75-86 variant had greatly reduced potency; (B) IC50 curves of myostatin and activin A for representative FS315-hFc hyperglycosylation variants. The three hyperglycosylated variants, K75N/C77T/K82T, C66A/K75N/C77T and C66S/K75N/C77T had moderate reduction in potency.

Figure 3. Heparin Binding Affinity Correlates to PK Property. Single 1 mg/kg intravenous administration of each heparin binding variant in mice (n=3): (A) The FS315-hFc variants plasma concentrations vs time following a single 1 mg/kg i.v. administration. The PK profiles showed that decreasing heparin-binding affinity correlated to progressively improved PK behavior (ND* indicates that there was no detectable heparin binding in the tested range for the variants). (B) Heparin binding affinity of the FS315-hFc variants, and the correlation to their serum clearance. Decreased heparin binding affinity results in reduced *in vivo* clearance (* indicates that there was no detectable heparin binding in the tested range for the variants).

Figure 4. Hyperglycosylation Resulted in a Molecular Weight and pI Shift. (A) Coomassie

blue staining of reduced FS315-hFc hyperglycosylation variants, which were separated by

polyacrylamide gel electrophoresis. Black arrows indicate the variants that showed a clear shift

in molecular weight due to hyperglycosylation. (B) cIEF profiles for two representative variants.

The hyperglycosylated variant K75N/C77T/K82T (in blue color) showed a clear acidic shift

compared to the non-hyperglycosylated variant K82T (in red color).

Figure 5. PK Profiles for FS315-hFc Hyperglycosylation Variants. Mice were given a single

dose of 1 mg/kg protein by intravenous administration (n=3 per group). The hyperglycosylated

variants K75N/C77T/K82T and C66A/K75N/C77T had significantly improved PK profiles over

the non-hyperglycosylated variant K82T, as well as wild type. The variant K75N/C77T/K82T

showed a comparable PK profile compared with the HBS deficient mutant ΔHBS.

Table 1. *In Vitro* Analytical Data for Heparin Binding Variants of FS315-hFc

The binding of recombinant FS315-hFc variants to heparin, myostatin or human neonatal Fc receptor (hFcRn) was determined by surface plasmon resonance (SPR). The binding affinities were measured and reported as the equilibrium dissociation constant (K_D). The charge heterogeneity of the variants was determined by capillary isoelectric focusing (cIEF), and shown as the range of isoelectric point (pI). The statistical parameters and analysis, including association constant (k_a) with S.E., dissociation constant (k_d) with S.E., and the average K_D values with S.D. (n=4 independent batches) for an internal control used in all SPR assays, are reported in Supplemental Table 3.

FS315-hFc Variant		Heparin Binding K_D (nM)	Myostatin Binding K_D (pM)	hFcRn Binding K_D (nM)	cIEF (pI)
Controls	wild type	0.2	20.2	31.4	5.07 - 5.89
	ΔHBS	ND*	17.4	48.0	4.82 - 5.72
	del75-86	ND*	57.1	38.8	4.83 - 5.26
One amino acid substitution	K84E	0.9	9.9	34.9	5.07 - 6.01
	K82E	1.5	11.9	10.5	5.48 - 6.09
Two amino acid substitution	K(76,84)E	0.8	9.0	33.0	4.87 - 5.95
	R78E/K84E	0.8	7.2	45.5	5.06 - 5.96
	K(75,76)E	1.1	11.7	34.2	5.05 - 5.26
	K(82,84)E	1.1	9.0	45.1	4.86 - 5.95
	R78E/K82E	1.3	3.9	53.3	4.96 - 5.96
	K(81,82)A	1.5	11.9	38.5	5.31 - 5.96
	K(76,82)E	3.9	10.5	38.2	4.89 - 5.26
	K(81,82)E	10.7	9.9	40.8	4.83 - 5.25
	K(81,82)D	20.6	7.1	24.7	4.88 - 5.59
Three amino acid substitution	K(76,81,82)A	9.4	11.3	41.6	5.24 - 5.93
	K(76,82,84)E	13.8	4.7	50.8	4.85 - 5.80
	K(76,81,82)E	ND*	4.2	44.0	4.87 - 5.80
	K(76,81,82)D	ND*	5.9	59.9	4.82 - 5.67

ND*: No detectable heparin binding in tested concentration ranges of 0.019 ~ 25nM FS315-hFc variants

Table 2. SMAD-responsive Luciferase Reporter Gene Assay

Recombinant FS315-hFc variants with either myostatin or activin A were incubated with A204 rhabdomyosarcoma cells stably expressing a SMAD-responsive luciferase reporter construct. The IC_{50} for each of the variants was determined by fitting the inhibition curve using Graphpad Prism software, and represented as mean ± S.D. (n=3).

FS315-hFc Variant	IC_{50} (nM) for Myostatin Stimulation	IC_{50} (nM) for Activin A Stimulation
wild type	0.6 ± 0.03	1.0 ± 0.02
Heparin Binding Variants		
ΔHBS	0.4 ± 0.02	1.4 ± 0.1
del75-86	> 10 *	> 10 *
K82E	0.6 ± 0.01	1.1 ± 0.02
K(81,82)E	0.6 ± 0.09	1.0 ± 0.2
R78E/K82E	0.5 ± 0.1	1.0 ± 0.1
K(82,84)E	0.7 ± 0.06	1.1 ± 0.01
K(76,82,84)E	0.4 ± 0.03	1.0 ± 0.1
K(76,81,82)A	0.8 ± 0.07	1.1 ± 0.1
K(76,81,82)E	0.6 ± 0.03	0.8 ± 0.01
K(76,81,82)D	0.7 ± 0.03	1.1 ± 0.1
Hyperglycosylation Variants		
K82T	0.9 ± 0.04	1.2 ± 0.04
G74N/K76S	0.9 ± 0.06	1.3 ± 0.06
K75N/C77T/K82T	1.8 ± 0.1	3.7 ± 0.6
C66A/K75N/C77T	1.5 ± 0.01	2.1 ± 0.05
C66S/K75N/C77T	1.9 ± 0.09	4.4 ± 1.2

*The IC_{50} curve was not saturated because of the weak binding

Table 3. PK Parameters for FS315-hFc Variants

CD-1 female mice (n=3 per group) were given a single dose of 1 mg/kg by intravenous administration.

Serum concentrations of the proteins were determined using an electro-chemiluminescent immunoassay,

and non-compartmental pharmacokinetic analysis PK parameters were calculated. Statistical parameters

S.E. and %CV as calculated by the sparse sampling method are shown for area under the curve (AUC).

FS315-hFc Variant	$T_{1/2}$ (h)	AUC (h*μg/ml)			CL (ml/h/kg)	V_{ss} (ml/kg)
		Mean	S.E.	%CV		
wild type	68.0	29.8	0.8	2.7	30.0	1600
ΔHBS	92.1	401.0	22.2	5.5	1.3	158
K82E	93.5	58.1	4.7	8.1	12.0	807
K82T	58.9	51.0	1.5	2.9	18.8	515
K(81,82)A	80.1	114.0	3.9	3.4	8.0	385
K(81,82)E	73.5	264.0	22.0	8.3	2.7	183
K(76,82)E	95.4	217.0	16.1	7.4	2.7	222
K(76,81,82)A	60.4	169.0	7.8	4.6	4.5	205
K(76,81,82)E	154.0	504.0	14.4	2.8	1.2	227
K(76,81,82)D	85.4	469.0	10.7	2.3	1.7	168
K75N/C77T/K82T	55.6	493.0	29.2	5.9	0.9	71
C66A/K75N/C77T	51.6	300.0	20.4	6.8	3.0	194

T½, terminal half-life; AUC, area under the curve; CL, clearance; V_{ss}, steady state volume of distribution

Table 4. Characterization of Endogenous and Hyperglycosylated N-linked

Glycosylation Sites. Percent glycan occupancy and sialic acid content are shown.

FS315-hFc Variant	Hyperglycosylation Site			N95		N112		N259	
	Location	Occupancy	Sialic Content[a]	Occupancy	Sialic Content[a]	Occupancy	Sialic Content[a]	Occupancy	Sialic Content[a]
wild type				14.7%	2.3	13.6%	0.9	96.0%	1.3
ΔHBS				22.7%	1.8	20.2%	1.7	98.8%	1.7
K82T	N80	n.d.	n.d.	49.7%	1.7	16.2%	0.8	97.1%	1.2
P85T	N83	n.d.	n.d.	9.3%	2.4	18.6%	1.1	97.0%	1.3
R78N/N80T	N78	n.d.	n.d.	31.3%	2.4	17.7%	1.0	97.0%	1.4
R86N/V88T	N86	[b]	[b]	21.0% [b]	1.0 [b]	15.1%	1.0	96.7%	1.1
G74N/K76T/P85T	N74	n.d.	n.d.	15.0%	2.2	23.1%	1.3	95.4%	1.3
	N83	n.d.	n.d.						
K75N/C77T/K82T	N75	69.7%	2.0	47.9%	2.3	16.9%	1.5	97.0%	1.4
	N80	n.d.	n.d.						
C66A/K75N/C77T	N75	39.6%	1.9	32.8%	2.3	17.8%	1.4	94.9%	1.3
C66S/K75N/C77T	N75	21.5%	2.0	32.9%	2.4	19.7%	1.4	95.1%	1.3

[a] mol sialic acid per mol oligosaccharide

[b] Results do not distinguish glycosylation at N86 or N95

Table 5. *In Vitro* Analytical Data for Hyperglycosylation Variants of FS315-hFc

The recombinant FS315-hFc variants with newly designed one or two consensus sequences (NXT/S) for N-glycosylation are listed in the table. The binding of the variants to heparin, myostatin or human neonatal Fc receptor (hFcRn) was determined by surface plasmon resonance (SPR). The binding affinities were measured and reported by the equilibrium dissociation constant (K_D). The charge heterogeneity of the variants was determined by capillary isoelectric focusing (cIEF), and shown as the range of isoelectric point (pI). The statistical parameters and analysis, including association constant (k_a) with S.E., dissociation constant (k_d) with S.E., and the average K_D values with S.D. (n = 4 independent batches) for an internal control used in all SPR assays, are reported in Supplemental Table 4.

FS315-hFc Variant	Heparin Binding K_D (nM)	Myostatin Binding K_D (pM)	hFcRn Binding K_D (nM)	cIEF (pI)
wild type	0.2	20.2	28.3	5.07 - 5.89
K82T	1.4	15.0	13.8	5.29 - 5.93
P85T	0.4	12.4	20.1	5.51 - 6.09
R78N/N80T	0.9	13.0	20.1	5.47 - 6.09
R86N/V88T	1.5	12.7	10.8	5.49 - 6.08
G74N/K76S	0.3	11.6	72.8	5.06 - 5.88
G74N/K76T	0.5	11.1	43.0	5.06 - 5.99
G74N/K76T/P85T	0.3	11.6	29.6	4.86 - 5.87
K75N/C77T/K82T	3.5	40.3	36.2	4.72 - 5.88
C66A/K75N/C77T	0.3	24.4	27.5	4.81 - 6.47
C66S/K75N/C77T	0.4	26.0	82.8	4.86 - 6.47
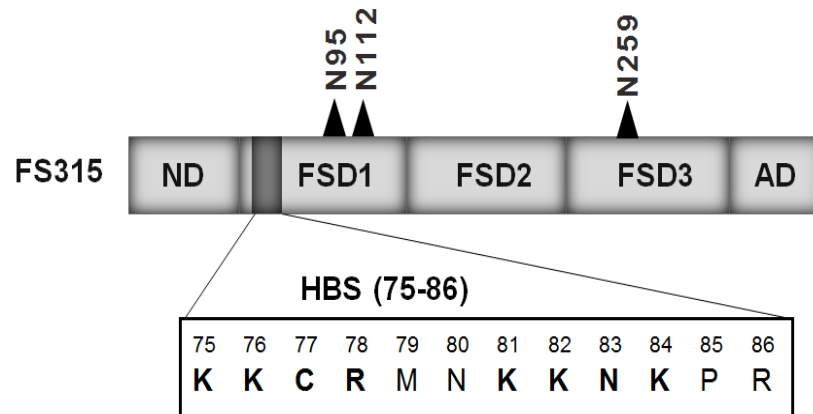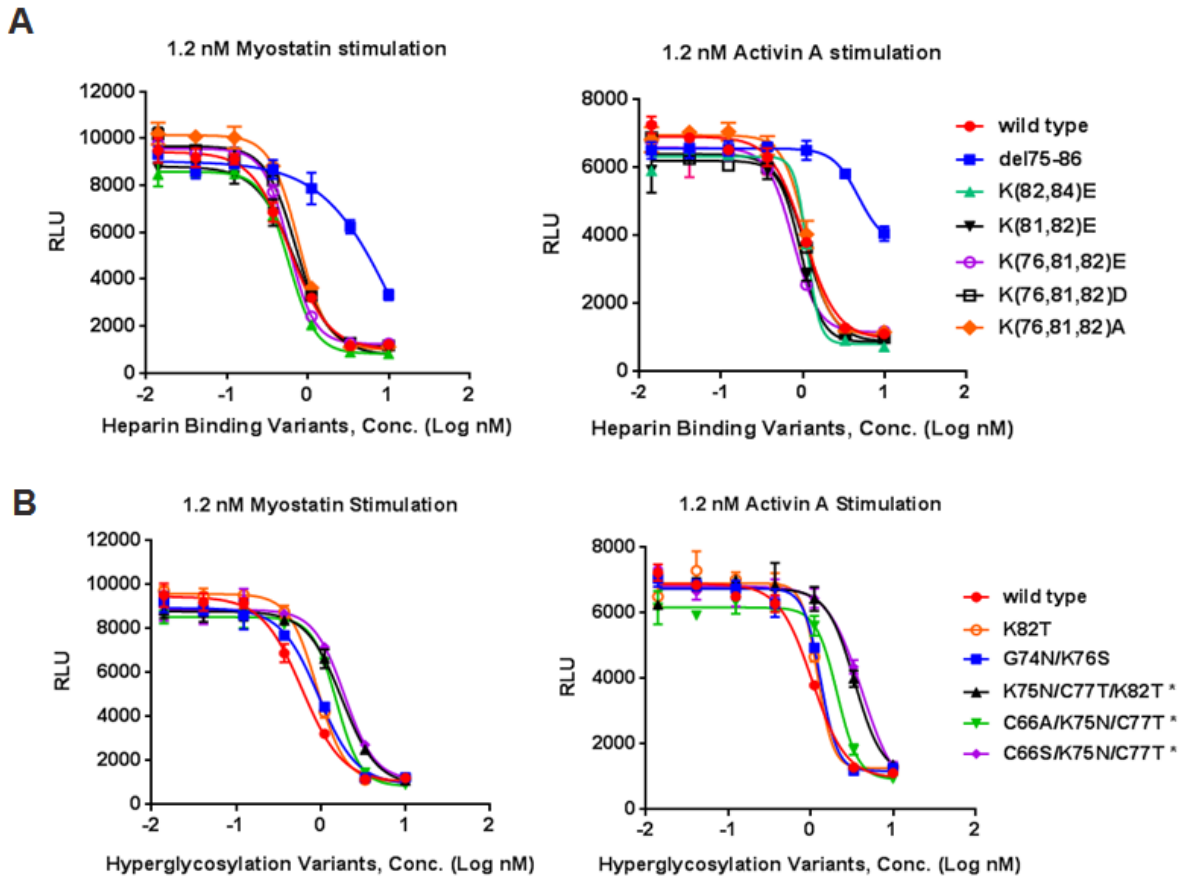
Figure 1

Figure 2

* Indicates hyperglycosylated FS315-hFc variants.

Figure 3
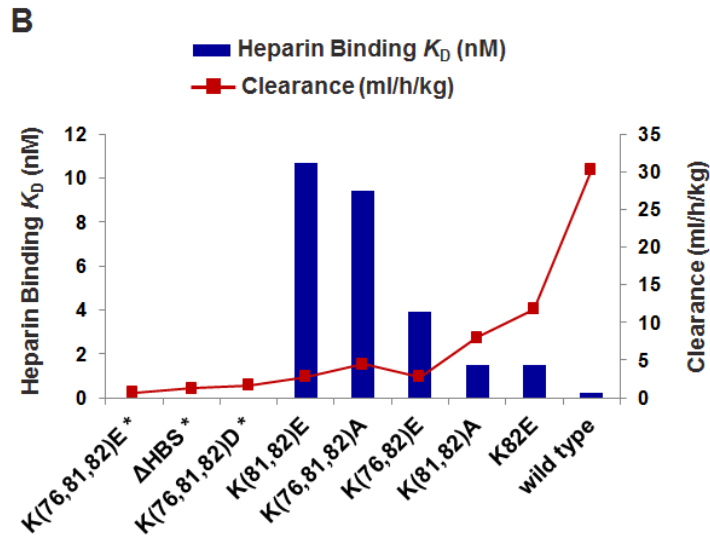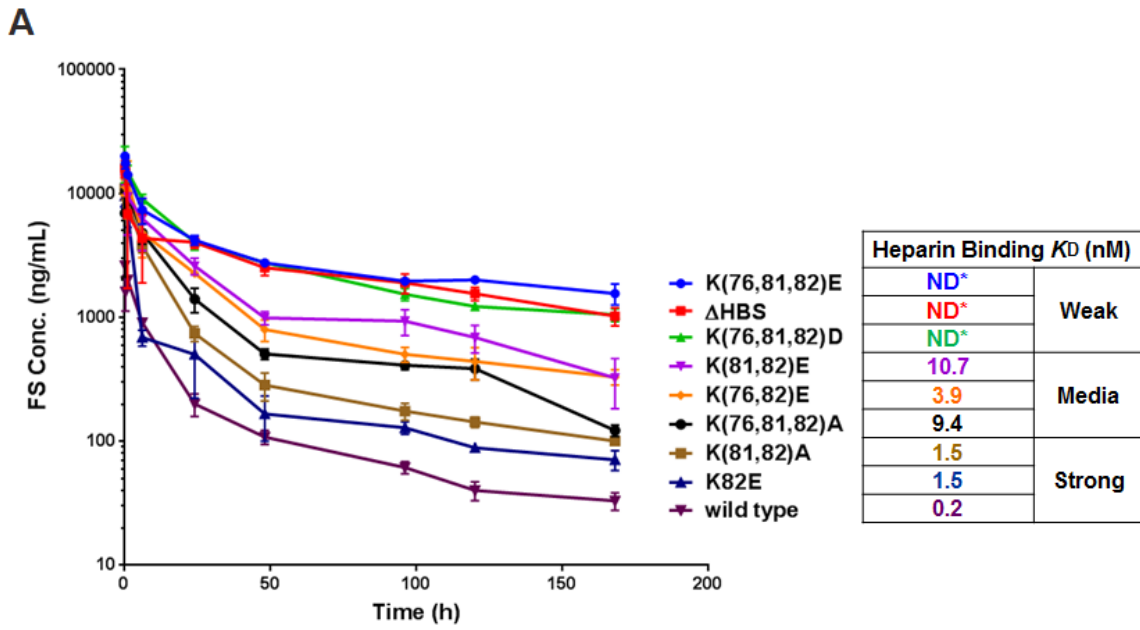
Figure 3
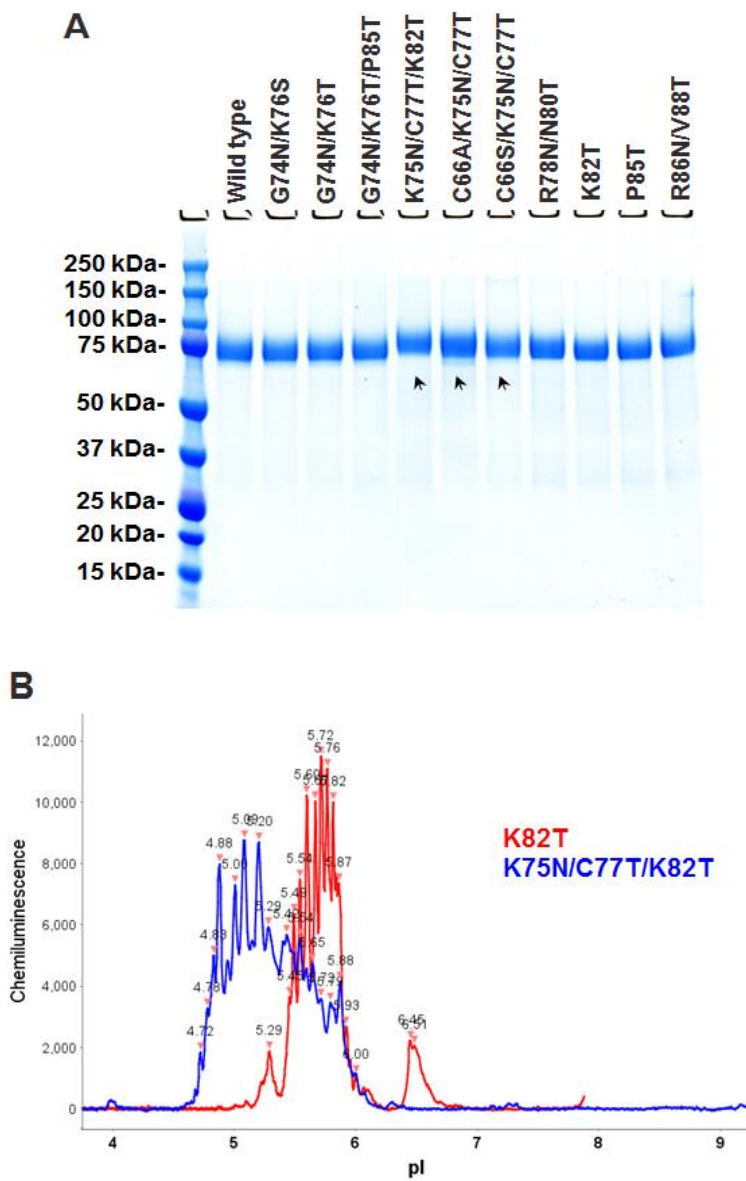
Figure 4
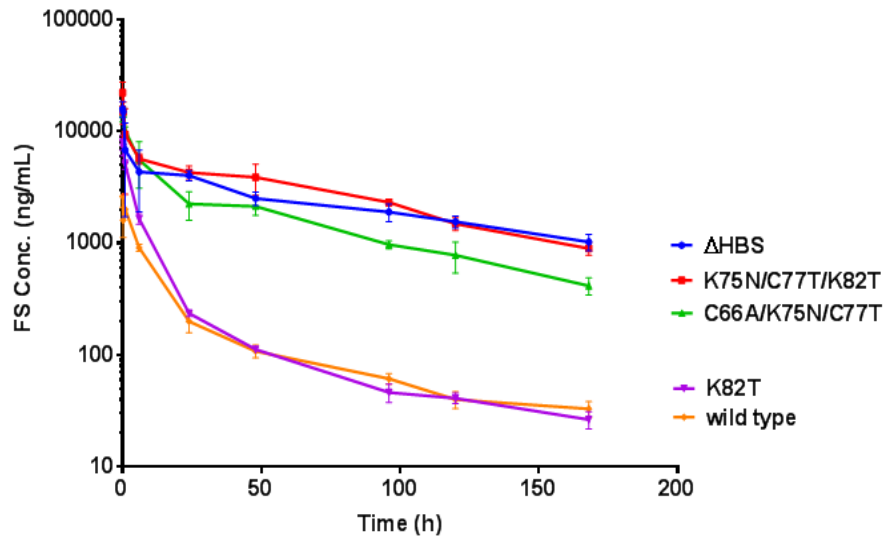
Figure 5

Supplemental Data

Protein Engineering on Human Recombinant Follistatin: Enhancing Pharmacokinetic Characteristics for Therapeutic Application

Chuan Shen, Andrea Iskenderian, Dianna Lundberg, Tao He, Kathleen Palmieri, Robert Crooker, Qingwei Deng, Matthew Traylor, Sheng Gu, Haojing Rong, David Ehmann, Brian Pescatore, Bettina Strack-Logue, Alla Romashko, George Baviello, John Gill, Bohong Zhang, Muthuraman Meiyappan, Clark Pan, Angela W. Norton

Supplementary Materials:

Supplemental Tables 1 to 4

Supplemental Figures 1 to 2

Protein Sequence for Human IgG1 Fc

Supplemental Table 1. Sequences within Heparin Binding Region for FS315-hFc Heparin Binding Variants. The sequences of the residues 73-88 in the heparin binding region for wild type, a core HBS replacement variant ΔHBS, a core HBS deletion variant del75-86, and a series of variants with point mutation(s) (shown as red) in the two basic BBXB motifs (shown as grey) are listed in the table.

FS315-hFc Variant	73	74	**75**	**76**	**77**	**78**	79	80	**81**	**82**	**83**	**84**	85	86	87	88
wild type	P	G	**K**	**K**	**C**	**R**	M	N	**K**	**K**	**N**	**K**	P	R	C	V
ΔHBS	P	G	S	T	C	V	V	D	Q	T	N	N	A	Y	C	V
del75-86	P	G													C	V
K82E	P	G	K	K	C	R	M	N	K	E	N	K	P	R	C	V
K84E	P	G	K	K	C	R	M	N	K	K	N	E	P	R	C	V
K(75,76)E	P	G	E	E	C	R	M	N	K	K	N	K	P	R	C	V
K(76,82)E	P	G	K	E	C	R	M	N	K	E	N	K	P	R	C	V
K(76,84)E	P	G	K	E	C	R	M	N	K	K	N	E	P	R	C	V
R78E/K82E	P	G	K	K	C	E	M	N	K	E	N	K	P	R	C	V
R78E/K84E	P	G	K	K	C	E	M	N	K	K	N	E	P	R	C	V
K(81,82)A	P	G	K	K	C	R	M	N	A	A	N	K	P	R	C	V
K(81,82)E	P	G	K	K	C	R	M	N	E	E	N	K	P	R	C	V
K(81,82)D	P	G	K	K	C	R	M	N	D	D	N	K	P	R	C	V
K(82,84)E	P	G	K	K	C	R	M	N	K	E	N	E	P	R	C	V
K(76,82,84)E	P	G	K	E	C	R	M	N	K	E	N	E	P	R	C	V
K(76,81,82)A	P	G	K	A	C	R	M	N	A	A	N	K	P	R	C	V
K(76,81,82)E	P	G	K	E	C	R	M	N	E	E	N	K	P	R	C	V
K(76,81,82)D	P	G	K	D	C	R	M	N	D	D	N	K	P	R	C	V

Supplemental Table 2. Sequences within Heparin Binding Region for FS315-hFc Hyperglycosylation Variants. The sequences of the residues 66-88 in the hyperglycosylation variants creating one or two consensus N-glycosylation sites (NXT/S) are listed in the table. The core heparin binding sequence is shown as red. The mutated residues are shown as bold, and created new N-glycosylation sites are shown as grey.

FS315-hFc Variant	66	67	68	69	70	71	72	73	74	**75**	**76**	**77**	**78**	79	80	**81**	**82**	**83**	**84**	85	86	87	88
Wild type	C	E	N	V	D	C	G	P	G	K	K	C	R	M	N	K	K	N	K	P	R	C	V
K82T	C	E	N	V	D	C	G	P	G	K	K	C	R	M	N*	K	T	N	K	P	R	C	V
P85T	C	E	N	V	D	C	G	P	G	K	K	C	R	M	N	K	K	N*	K	T	R	C	V
R78N/N80T	C	E	N	V	D	C	G	P	G	K	K	C	N*	M	T	K	K	N	K	P	R	C	V
R86N/V88T	C	E	N	V	D	C	G	P	G	K	K	C	R	M	N	K	K	N	K	P	N*	C	T
G74N/K76S	C	E	N	V	D	C	G	P	N*	K	S	C	R	M	N	K	K	N	K	P	R	C	V
G74N/K76T	C	E	N	V	D	C	G	P	N*	K	T	C	R	M	N	K	K	N	K	P	R	C	V
G74N/K76T/P85T	C	E	N	V	D	C	G	P	N*	K	T	C	R	M	N	K	K	N*	K	T	R	C	V
K75N/C77T/K82T	C	E	N	V	D	C	G	P	G	N*	K	T	R	M	N*	K	T	N	K	P	R	C	V
C66A/K75N/C77T	**A**	E	N	V	D	C	G	P	G	N*	K	T	R	M	N	K	K	N	K	P	R	C	V
C66S/K75N/C77T	**S**	E	N	V	D	C	G	P	G	N*	K	T	R	M	N	K	K	N	K	P	R	C	V

*: Asparagine residues for hyperglycosylation

Supplemental Table 3. *In Vitro* **Analytical Data for Heparin Binding Variants of FS315-hFc.** The binding of FS variants to heparin, myostatin or hFcRn was determined by surface plasmon resonance (SPR). The binding affinities were measured and reported as the equilibrium dissociation constant (K_D). The charge heterogeneity of the variants were determined by capillary isoelectric focusing (cIEF), and shown as the range of isoelectric point (pI). Association constant (k_a) with S.E. and dissociation constant (k_d) with S.E. for each of K_D values, and the average K_D values with S.D. (n = 4 independent experiments) for an internal control used in all SPR assays are included.

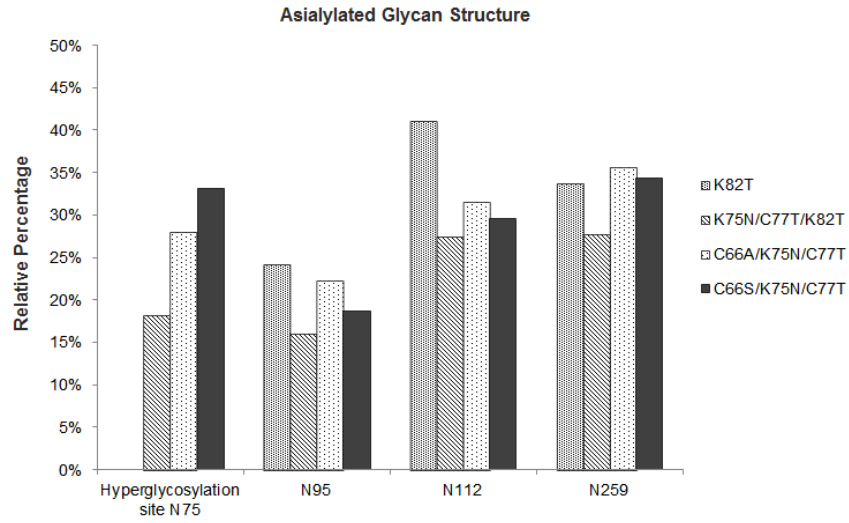| FS315-hFc Variant		Heparin Binding			Myostatin Binding			hFcRn Binding			cIEF (pI)
		k_a (M^{-1}s^{-1}) X 10^5 (S.E.)	k_d (s^{-1}) X10^{-4} (S.E.)	K_D (nM)	k_a (M^{-1}s^{-1}) X 10^5 (S.E.)	k_d (s^{-1}) X10^{-7} (S.E.)	K_D (pM)	k_a (M^{-1}s^{-1}) X 10^5 (S.E.)	k_d (s^{-1}) X10^{-4} (S.E.)	K_D (nM)	
Controls	wild type	61.9 (0.6)	10.4 (0.2)	0.2	36.6 (0.2)	741.0 (3.7)	20.2	2.0 (0.02)	61.8 (0.4)	31.4	5.07 - 5.89
	ΔHBS	ND*	ND*	ND*	62.7 (0.6)	1091.0 (7.5)	17.4	2.6 (0.02)	125.6 (1.1)	48.0	4.82 - 5.72
	del75-86	ND*	ND*	ND*	34.4 (0.06)	1970.0 (7.5)	57.1	1.1 (0.004)	42.7 (0.07)	38.8	4.83 - 5.26
One amino acid substitution	K84E	21.3 (0.06)	18.2 (0.06)	0.9	81.7 (0.4)	810.0 (4.2)	9.9	1.9 (0.02)	65.4 (0.4)	34.9	5.07 - 6.01
	K82E	20.2 (0.2)	29.9 (0.3)	1.5	61.7 (0.7)	737.0 (1.0)	11.9	2.5 (0.03)	75.6 (0.8)	30.7	5.48 - 6.09
Two amino acid substitution	K(76,84)E	14.7 (0.03)	11.5 (0.04)	0.8	76.0 (0.3)	680.0 (3.5)	9.0	1.8 (0.03)	58.6 (0.4)	33.0	4.87 - 5.95
	R78E/K84E	15.9 (1.0)	13.2 (0.1)	0.8	84.5 (0.4)	610.0 (3.2)	7.2	1.2 (0.002)	56.5 (0.08)	45.5	5.06 - 5.96
	K(75,76)E	25.8 (0.3)	28.5 (0.3)	1.1	71.7 (0.9)	838.0 (1.2)	11.7	1.5 (0.006)	52.5 (0.09)	34.2	5.05 - 5.26
	K(82,84)E	9.8 (0.02)	10.6 (0.04)	1.1	92.2 (0.5)	826.0 (4.2)	9.0	1.4 (0.02)	63.3 (0.4)	45.1	4.86 - 5.95
	R78E/K82E	10.7 (0.5)	14.0 (0.1)	1.3	89.4 (0.7)	350.0 (6.2)	3.9	1.7 (0.04)	88.4 (2.1)	53.3	4.96 - 5.96
	K(81,82)A	17.3 (0.2)	26.9 (0.3)	1.5	72.1 (0.5)	859.0 (7.5)	11.9	1.8 (0.02)	69.3 (0.6)	38.5	5.31 - 5.96
	K(76,82)E	6.7 (0.08)	24.1 (0.3)	3.9	64.9 (0.7)	679.0 (1.0)	10.5	3.5 (0.06)	133.2 (2.2)	38.2	4.89 - 5.26
	K(81,82)E	2.0 (0.06)	21.4 (0.5)	10.7	72.0 (0.8)	711.0 (1.1)	9.9	2.8 (0.03)	115.8 (1.2)	40.8	4.83 - 5.25
	K(81,82)D	1.5 (0.01)	31.8 (0.1)	20.6	90.1 (0.6)	639.0 (2.8)	7.1	2.9 (0.01)	71.3 (0.2)	24.7	4.88 - 5.59
Three amino acid substitution	K(76,81,82)A	4.1 (0.09)	38.4 (0.5)	9.4	72.2 (0.3)	818.0 (4.5)	11.3	1.5 (0.02)	63.9 (0.5)	41.6	5.24 - 5.93
	K(76,82,84)E	1.1 (0.01)	15.0 (0.05)	13.8	91.6 (0.5)	434.0 (3.8)	4.7	1.6 (0.04)	83.9 (1.4)	50.8	4.85 - 5.80
	K(76,81,82)E	ND*	ND*	ND*	41.3 (0.2)	172.0 (1.6)	4.2	3.1 (0.06)	138.0 (2.5)	44.0	4.87 - 5.80
	K(76,81,82)D	ND*	ND*	ND*	73.9 (0.4)	437.0 (1.6)	5.9	5.3 (0.1)	318.8 (8.5)	59.9	4.82 - 5.67
Internal control		K_D (nM) 0.4 ± 0.06			K_D (pM) 4.5 ± 0.3			K_D (nM) 23.5 ± 1.9			5.51 - 6.17

ND*: No detectable heparin binding in tested concentration ranges of 0.019 ~ 25nM FS315-hFc variants

Supplemental Table 4. *In Vitro* **Analytical Data for Hyperglycosylation Variants of FS315-hFc.** The binding of FS variants to heparin, myostatin or hFcRn was determined by surface plasmon resonance (SPR). The binding affinities were measured and reported as the equilibrium dissociation constant (K_D). The charge heterogeneity of the variants were determined by capillary isoelectric focusing (cIEF), and shown as the range of isoelectric point (pI). Association constant (k_a) with S.E. and dissociation constant (k_d) with S.E. for each of K_D values, and the average K_D values with S.D. (n = 4 independent experiments) for an internal control used in all SPR assays are included.

FS315-hFc Variant	Heparin Binding			Myostatin Binding			hFcRn Binding			cIEF (pI)
	k_a (M^{-1}s^{-1}) X 10^5 (S.E.)	k_d (s^{-1}) X10^{-4} (S.E.)	K_D (nM)	k_a (M^{-1}s^{-1}) X 10^5 (S.E.)	k_d (s^{-1}) X10^{-7} (S.E.)	K_D (pM)	k_a (M^{-1}s^{-1}) X 10^5 (S.E.)	k_d (s^{-1}) X10^{-4} (S.E.)	K_D (nM)	
wild type	61.9 (0.6)	10.4 (0.2)	0.2	36.6 (0.2)	741.0 (3.7)	20.2	1.8 (0.006)	50.1 (0.09)	28.3	5.07 - 5.89
K82T	22.8 (0.2)	32.8 (0.3)	1.4	62.8 (0.5)	945.0 (8.1)	15.0	3.4 (0.02)	46.3 (0.2)	13.8	5.29 - 5.93
P85T	60.6 (0.6)	22.6 (0.2)	0.4	66.7 (0.1)	827.0 (1.8)	12.4	2.3 (0.007)	47.1 (0.08)	20.1	5.51 - 6.09
R78N/N80T	30.3 (0.3)	25.6 (0.3)	0.9	64.1 (0.08)	834.0 (1.2)	13.0	4.0 (0.008)	41.8 (0.07)	20.1	5.47 - 6.09
R86N/V88T	18.8 (0.2)	24.5 (0.3)	1.5	71.1 (0.1)	904.0 (1.4)	12.7	5.7 (0.05)	62.0 (0.5)	10.8	5.49 - 6.08
G74N/K76S	48.7 (0.1)	15.1 (0.05)	0.3	61.3 (0.2)	710.0 (3.6)	11.6	0.6 (0.005)	44.3 (0.09)	72.8	5.06 - 5.88
G74N/K76T	43.4 (0.2)	20.7 (0.09)	0.5	58.6 (0.2)	650.0 (2.9)	11.1	1.6 (0.05)	67.9 (1.9)	43.0	5.06 - 5.99
G74N/K76T/P85T	54.5 (0.1)	15.8 (0.04)	0.3	85.4 (0.7)	988.0 (5.8)	11.6	1.3 (0.01)	38.5 (0.3)	29.6	4.86 - 5.87
K75N/C77T/K82T	10.5 (0.07)	35.7 (0.4)	3.5	30.4 (0.03)	1230.0 (3.6)	40.3	1.0 (0.006)	36.5 (0.09)	36.2	4.72 - 5.88
C66A/K75N/C77T	32.1 (0.05)	10.7 (0.03)	0.3	46.9 (0.3)	1140.0 (7.8)	24.4	1.1 (0.009)	30.1 (0.2)	27.5	4.81 - 6.47
C66S/K75N/C77T	27.4 (0.04)	11.5 (0.04)	0.4	45.6 (0.4)	1180.0 (8.4)	26.0	1.6 (0.07)	132.5 (0.4)	82.8	4.86 - 6.47
Internal control	K_D (nM) 0.4 ± 0.06			K_D (pM) 4.5 ± 0.3			K_D (nM) 23.5 ± 1.9			5.51 - 6.17
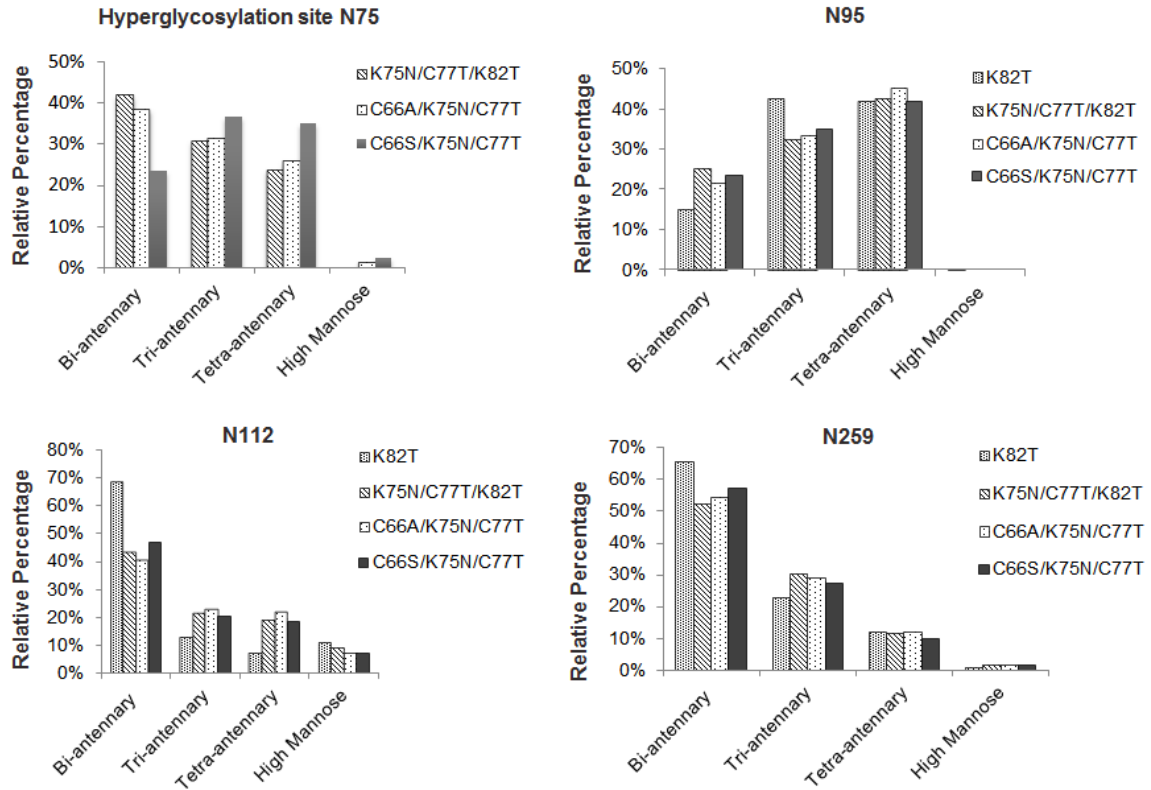
Supplemental Figure 1. Comparison of the relative abundance of the antennary structures at observed N-linked sites in non-hyperglycosylated variant K82T, and three hyperglycosylated variants K75N/C77T/K82T, C66A/K75N/C77T and C66S/K75N/C77T. The amount of each antennary structure is presented as a relative abundance of oligosaccharide species relative to the total oligosaccharide measured at a given site.

Asialylated Glycan Structure

Legend: K82T, K75N/C77T/K82T, C66A/K75N/C77T, C66S/K75N/C77T

X-axis categories: Hyperglycosylation site N75, N95, N112, N259

Y-axis: Relative Percentage

Supplemental Figure 2. Comparison of the relative abundance of the asialylated glycan structures at each of the N-linked sites in non-hyperglycosylated variant K82T and three hyperglycosylated variants K75N/C77T/K82T, C66A/K75N/C77T and C66S/K75N/C77T. The amount of asialylated glycan structures is presented as the relative abundance of oligosaccharide species without terminal sialic acid relative to the total oligosaccharide measured at a given site.

Protein Sequence for Human IgG1 Fc

DKTHTCPPCPAPELLGGPSVFLFPPKPKDTLMISRTPEVTCVVVDVSHEDPEVKFNWYVDGVE

VHNAKTKPREEQYNSTYRVVSVLTVLHQDWLNGKEYKCKVSNKALPAPIEKTISKAKGQPREP

QVYTLPPSRDELTKNQVSLTCLVKGFYPSDIAVEWESNGQPENNYKTTPPVLDSDGSFFLYSK

LTVDKSRWQQGNVFSCSVMHEALHNHYTQKSLSLSPGK